WATER RESOURCES RESEARCH, VOL. 49, 1446–1457, doi:10.1002/wrcr.20135, 2013

Seasonal small-scale spatial variability in alpine snowfall and snow accumulation

D. E. Scipión,[1] R. Mott,[2] M. Lehning,[2,3] M. Schneebeli,[1] and A. Berne[1]

Received 30 May 2012; revised 18 December 2012; accepted 5 February 2013; published 12 March 2013.

[1] In mountainous regions, snow accumulation on the ground is crucial for mountain hydrology and water resources. The present study investigates the link between the spatial variability in snowfall and in snow accumulation in the Swiss Alps. A mobile polarimetric X-band radar deployed in the area of Davos (Switzerland) collected valuable and continuous information on small-scale precipitation for the winter seasons of 2009/2010 and 2010/2011. Local measurements of snow accumulation were collected with airborne laser-scanning for the winters of 2007/2008 and 2008/2009. The spatial distribution of snow accumulation exhibits a strong interannual consistency that can be generalized over the winters in the area. This unique configuration makes the comparison of the variability in total snowfall amount estimated from radar and in snow accumulation possible over the diverse winter periods. As expected, the spatial variability, quantified by means of the variogram, is shown to be larger in snow accumulation than in snowfall. However, the variability of snowfall is also significant, especially over the mountain tops, leads to preferential deposition during snowfall and needs further investigation. The higher variability at the ground is mainly caused by snow transport.

Citation: Scipión, D. E., R. Mott, M. Lehning, M. Schneebeli, and A. Berne (2013), Seasonal small-scale spatial variability in alpine snowfall and snow accumulation, *Water Resour. Res.*, *49*, 1446–1457, doi:10.1002/wrcr.20135.

1. Introduction

[2] Snowfall and resulting snow accumulation in mountainous terrain are crucial for studying and predicting natural hazards like floods and avalanches, as well as for water resources, hydroelectric power, and tourism (e.g., ski resorts). At local scales, the spatial variability in both snowfall and snow accumulation is governed by the interaction among cloud microphysics, atmospheric dynamics, and topographic features [*Roe*, 2005; *Pomeroy et al*., 1997; *Lehning et al*., 2008; *Zängl et al*., 2008; *Schirmer et al*., 2011]. These processes make the distribution of snow accumulation a complex and dynamic process [*Mott et al*., 2011b]. The spatial variability of snow accumulation is important in order to estimate the timing of the snow melt [*Luce et al*., 1998; *Grünewald et al*., 2010] and to forecast avalanche danger [*Birkeland et al*., 1995; *Schweizer et al*., 2003]. *Lehning et al*. [2008] have proposed the concept of preferential deposition, i.e., "the spatially varying deposition of precipitation due to topography-induced flow field modification close to the surface" as an important driver of accumulation distribution. This concept has been studied and evaluated using measured snow deposition fields, simulated precipitation, and wind fields [*Mott et al*., 2010; *Dadic et al*., 2010], but no direct measured precipitation fields were available for verification. *Lehning et al*. [2011] studied the effect of the roughness of the terrain in snow deposition using high-resolution snow accumulation measurements.

[3] Estimating snowfall rate with radars is difficult because snowflakes are easily transported by wind, and their density varies from event to event. Weather radars provide high resolution but indirect measurements of snowfall. The use of weather radar for snow studies has become more popular in the last decade, and the areas of research are diverse. A study of snowfall rate based on radar reflectivity was made by *Matrosov* [1992] using X- and Ka-band radars. Later, *Matrosov* [1998] generalized the technique and verified the findings with local snow accumulation measurements. However, the technique was sensitive to changes in snow density, which can cause an overestimation in the snowfall by a factor of four. *Kneifel et al*. [2011] also performed studies of snowfall by using two radars, one frequency modulated-continuous wave operating at 24.1 GHz and a 35.5 GHz cloud radar. They collected 6 months of collocated measurements and estimated snow accumulation. Measurement of snowfall using a polarimetric X-band radar was studied by *Matrosov et al*. [2009]. In their study, they relied on snowflake shape models and snowflake size distribution to calculate the snowfall precipitation rate. However, small changes in the snow density could again lead to significant estimation errors. Radar data can also be

[1]Environmental Remote Sensing Laboratory (LTE), School of Architecture, Environmental and Civil Engineering (ENAC), École Polytechnique Fédérale de Lausanne (EPFL), Lausanne, Switzerland.
[2]WSL–Institute for Snow and Avalanche Research (SLF), Davos, Switzerland.
[3]Laboratory of Cryospheric Sciences (CRYOS), School of Architecture, Environmental and Civil Engineering (ENAC), École Polytechnique Fédérale de Lausanne (EPFL), Lausanne, Switzerland.

Corresponding author: D. E. Scipión, EPFL ENAC IIE LTE, GR C2 565 (Bâtiment GR), Station 2, Lausanne CH-1015, Switzerland. (danny.scipion@epfl.ch)

0043-1397/13/10.1002/wrcr.20135

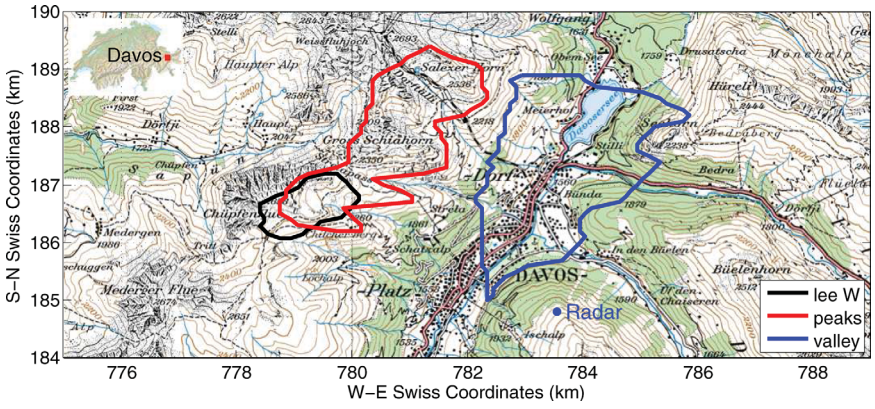

Figure 1. Study area near Davos, Switzerland. The colored lines represent the different subdomains of interest. The lee-W subdomain is delineated in black and corresponds to the leeward side of the Wannengrat. The other subdomains are peaks and valley which can be found in red and blue, respectively. The location of the radar is marked with a blue dot.

used to investigate the microphysical processes occurring during snow fall [*Evans et al*., 2005; *Mitchell et al*., 2006; *Kennedy and Rutledge*, 2011; *Schneebeli et al*., 2013]. Estimations of snowfall rate and/or snow accumulation are sensitive to information that is difficult to measure, such as snowflake density and snowflake distribution [e.g., *Matrosov et al*., 2009].

[4] In order to understand the contribution of snow precipitation on snow distribution variability on the ground, the main objective of this paper is to compare and analyze the respective spatial variability in snowfall and snow accumulation over the same area. These comparisons and analyses are based on using snowfall observations collected by a Doppler dual-polarization X-band radar deployed in the eastern Swiss Alps and snow accumulation measurements from laser scans. This unique combination of high spatial resolution data allows the analysis of small-scale variability, which is important in regions with complex topography. In addition, the influence of the topographically induced flow pattern is investigated by considering subdomains over which the radar beam is at distinct altitude ranges.

[5] This paper is organized as follows. Section 2 presents a description of the different data sets for snow accumulation and radar measurements used in this study. Additionally, the description of the different domains is presented along with the analysis methods. The methodology of the analyses is presented in section 3. Results from the different domains and measurements are presented in section 4. Section 5 summarizes the findings and mentions future work.

2. Experimental Setup

2.1. Site Description

[6] Davos is a Swiss city located at 1560 m above sea level (asl) in the Eastern Swiss Alps and hosts the WSL Institute for Snow and Avalanche Research SLF. The Wannengrat experimental site near Davos provides useful data for snow-cover- and hydrology-related research [*Grünewald et al*., 2010; *Mott et al*., 2010; *Bellaire and Schweizer*, 2011; *Schirmer et al*., 2011; *Mott et al*., 2011b]. The potential of the area for snowfall studies was reinforced with the installation of a mobile X-band dual-polarization weather radar (MXPol) in the vicinity of Davos (see Figure 1) between 2009 and 2011.

2.2. Snow Accumulation Measurements

[7] Snow accumulation measurements for this study were obtained using airborne laser scans (ALS, see Figure 2), located mainly in the Wannengrat area. The ALS measurements of snow accumulation were obtained at the time of peak accumulation, which also corresponds to the end of the accumulation, for the winter seasons of 2007/2008 and 2008/2009 [*Mott et al*., 2010; *Schirmer et al*., 2011]. Unfortunately, the two snow accumulation periods do not coincide with the MXPol measurements because the latter was installed at the end of September 2009.

[8] The studies in the area revealed that snow depth measurements at time of peak accumulation of these two consecutive winters have a strong interannual consistency of snow depths [*Schirmer et al*., 2011]. This quantitative interannual consistency was generalized for all winter events in the area [*Schirmer et al*., 2011]. Similarities in snow distribution, particularly in its spatial variability, can be assumed at the end of each winter season. This makes the comparison of the variability in snow accumulation and snowfall for different winter periods still meaningful.

2.3. Radar Measurements

[9] MXPol was deployed in the vicinity of Davos, Switzerland (see Figure 1) at the beginning of the winter season of 2009. MXPol specifications and parameters are presented in Table 1. Since its installation, the radar recorded preprocessed data of magnitude and phase for the vertical and horizontal polarizations, which allowed the calculation of the different polarimetric radar variables. The first variable used in the present study is the radar reflectivity at horizontal polarization (Z_H), which is related to the amount and type of hydrometeors in the radar sampling volume. The radar reflectivity Z_H can be expressed as a function of the particle size distribution $N(D)$ ($\mathrm{m}^{-3}\ \mathrm{mm}^{-1}$):

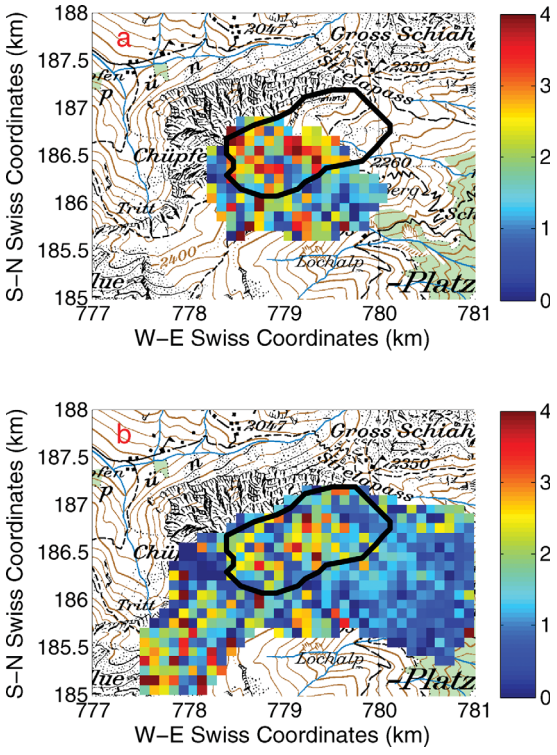

Figure 2. Snow accumulation measurements obtained from ALS in the Wannengrat area resampled at 100 m resolution: (a) measurements from the 2007/2008 period and (b) measurements from the 2008/2009 period. The lee-W domain is highlighted in black.

$$Z_H = \frac{4\lambda^4 10^6}{\pi^4 |K_w|^2} \int_{D_{\min}}^{D_{\max}} N(D)\sigma_{B_H}(D)\mathrm{d}D, \qquad (1)$$

where σ_{B_H} is the backscattering cross section at the horizontal polarization (cm^2) of a particle with an equivolume diameter D (mm). λ (cm) represents the radar wavelength and K_w is the dielectric factor for liquid water. In the case of snow or ice particles, the radar reflectivity needs to be corrected by the factor $|K_i|^2/|K_w|^2$, where $|K_i|^2$ represents the dielectric factor for ice.

Table 1. Mobile X-Band Radar: Specifications[a]

Quantity	Value
Radar type	Pulsed
Frequency	9.41 GHz
Wavelength	0.0319 m
Transmitter power	7.5 kW/channel
Receiver	Dual polarization (simultaneous)
Processing	DPP (staggered PRT)
Pulse repetition times (PRT)	950–1200 μs
Aliased velocity	~31.5 m s^{-1}
Angular resolution	~1°
Pulse width	0.5 μs
Range resolution	75 m
Maximum range	40 km
Scanning sequence	4 PPI scans (0°, 2°, 5°, 9°), 1 range height indicator (RHI) scan (18° azimuth), 3 PPI scans (14°, 20°, 27°), 1 RHI scan
Total scan time	5 min

[a]Adapted from *Schneebeli and Berne* [2012].

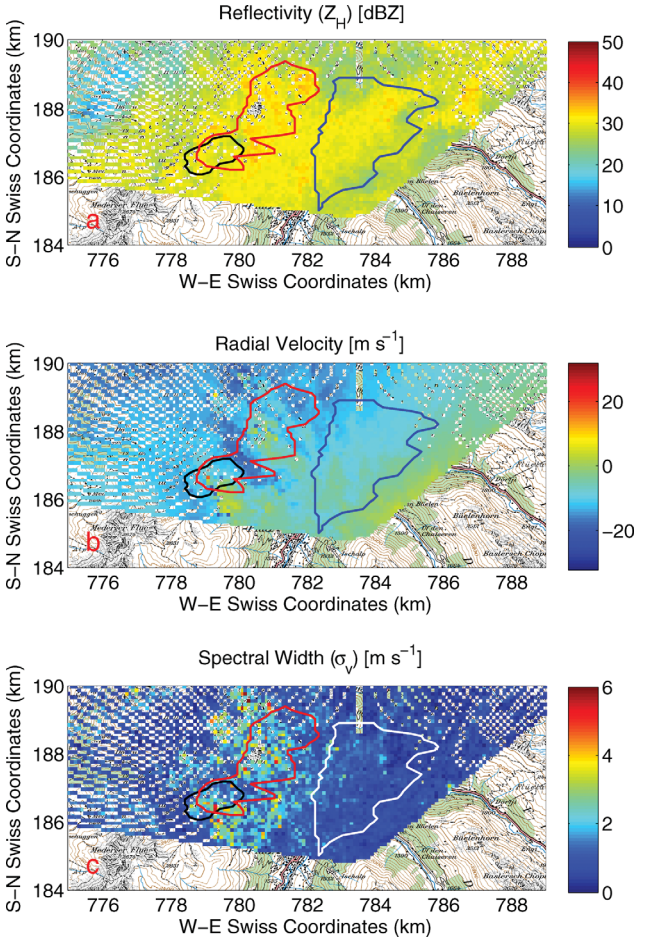

Figure 3. Radar measurements on 18 March 2011 at 0006:48 UTC: (a) reflectivity at the horizontal polarization, (b) radial velocity, and (c) Doppler spectral width. The different domains are delineated in different colors for better readability.

[10] The second variable in the study is the mean Doppler radial velocity v_r (m s^{-1}), which is an indicative of the average scatterer's radial velocity. Finally, the third variable used in the study is the Doppler spectral width σ_v (m s^{-1}), which is related to shear or turbulence within the resolution volume [*Doviak and Zrnić*,] and can be expressed as

$$\sigma_v^2 = \sigma_s^2 + \sigma_\alpha^2 + \sigma_d^2 + \sigma_0^2 + \sigma_t^2. \qquad (2)$$

[11] Equation (2) shows that the measured spectral width (σ_v^2) results from the contribution of many factors such as shear (σ_s^2), antenna motion (σ_α^2), different speeds of fall for different sized hydrometeors (σ_d^2), change in orientation or vibration of hydrometeors (σ_0^2), and turbulence (σ_t^2). Consequently, the spectral width due to turbulence (σ_t^2) is contaminated by all the other factors. In the subdomains of study, the antenna motion is the same. The effect of the shear in the spectral width is minimal over the time of analysis. Finally, because we do not expect significant changes in the snow particles, broadening due to fall speed and

Table 2. Radar Winter Events

Period	Days Interval	Days of Snowfall	Total Amount at Weissfluhjoch (mm)
2009/2010	8 Oct 2009–27 Mar 2010	49 days	458
Mar. 2011	17–20 Mar 2011	4 days	49

orientation can also be assumed as constant. As a result, the variations in the measured spectral width are assumed to be mainly due to turbulence. An example of Z_H, v_r, and σ_v measurements is presented in Figure 3.

[12] MXPol was removed from Davos in July 2011 for upgrades and maintenance, but its database contains the significant snow events of the winters of 2009/2010 and one of 2010/2011. In the winter of 2009/2010 the number of snow days registered by the radar corresponds to 49. Unfortunately, during the 2010/2011 winter the number of days with snow corresponds to 10, which is not representative of the whole winter season. Nevertheless, a significant event with predominant NW winds was registered in March 2011 and is included in this study. A summary of the considered periods is presented in Table 2, along with the total snowfall measured at the Weissfluhjoch station located approximately at 1 km from the Wannengrat area.

[13] Snow accumulation measurements from the Wannengrat area are studied together with estimates of total snowfall water equivalent obtained from radar reflectivity (Z_H). Estimates of Doppler spectral width (σ_v), also obtained from MXPol, are used to study the intensity of turbulence within the resolution volume.

2.4. Z-S Relations

[14] As explained in section 1, there is a significant uncertainty associated with radar estimation of snowfall rate. The most common $Z_H = aS^b$ relations in snow from X-band radar are listed in Table 3 and illustrated in Figure 4. The different colors represent the different studies from which they were obtained. Some of the relations were based on snow particle size spectra information [e.g., *Matrosov et al*., 2009] and assumed densities, others on simulations at different frequencies [e.g. *Matrosov*, 1992], and others on synchronous measurements of the snowfall reflectivity and their corresponding water equivalent [e.g., *Fujiyoshi et al*., 1990; *Boucher and Wieler*, 1985].

[15] Because the radar was not 100% operational over the two winter seasons while it was deployed in the Davos area, it is more than likely that there are missing events (days or weeks) from the radar database. As a consequence, a comparison of total snowfall amount (expressed in millimeters of liquid water) and snow accumulation on the ground is unrealistic. The purpose of this study is to analyze the spatial distribution in snow accumulation and in total snowfall amount under the main assumption that the events that had more impact in snow accumulation are part of the radar's database.

[16] Different *Z-S* relations have been tested in this study and led to very similar results in terms of spatial distribution of snowfall obtained from the radar. The discrepancies observed were in the estimation of total amounts of snowfall at each method. In the end, the *Z-S* relation presented by *Boucher and Wieler* [1985] was selected because it is based on direct observations, and the curve lies close to the median of the all *Z-S* relation presented in Figure 4.

2.5. Domains of Analysis

2.5.1. Wannengrat Area

[17] The leeward area of the Wannengrat ("lee-W," delineated in Figure 1) was selected due to local snow accumulation measurements and radar coverage. Snow deposition on the leeward area of the Wannengrat is directly affected by the NW winds [*Mott et al*., 2010; *Schirmer et al*., 2011], and it was already demonstrated by *Mott et al*. [2010] that small-scale precipitation patterns drive snow deposition here. Additionally, the laser scan measurements were located predominantly in this area (see Figure 2), and the Wannengrat area is permanently equipped with seven weather stations. The elevations of the lee-W subdomain vary from 2300 to 2700 masl (see Figure 5a). The subdomain is illustrated on a grid that corresponds to the Swiss coordinates, and the elevations are based on the Swiss digital elevation model (DEM) [*Swisstopo*, 2004]. The area of the subdomain corresponds to 1.5 km^2.

[18] The radar sequence of the plane position indicator (PPI) had seven elevations which start at 0° (see Table 1). Nevertheless, the first three elevations (0°, 2°, and 5°) were strongly contaminated by ground clutter (GC) returns, especially when the beam pointed close to the Wannengrat area. The PPI at 9° elevation is used in this study because it

Table 3. X-band Snowfall (*S*) and Reflectivity (*Z*) Relations[a]

Relation	*a*	*b*	Additional Info
Boucher and Wieler [1985]	229	1.65	
Fujiyoshi et al. [1990]	427	1.09	
Puhakka [1975]	1050	2.00	
Sekhon and Srivastava [1970]	1780	2.21	
Matrosov [1992] (a)	410	1.60	Snow density = 0.02 g cm^{-3}
Matrosov [1992] (b)	340	1.75	Snow density = 0.04 g cm^{-3}
Matrosov [1992] (c)	240	1.95	Snow density = 0.06 g cm^{-3}
Matrosov et al. [2009] B90A	67	1.28	SSD data set: *Braham* [1990]
Matrosov et al. [2009] B90B	114	1.39	SSD data set: *Braham* [1990]
Matrosov et al. [2009] B90C	136	1.20	SSD data set: *Braham* [1990]
Matrosov et al. [2009] W08A	28	1.44	SSD data set: *Woods et al*. [2008]
Matrosov et al. [2009] W08B	36	1.56	SSD data set: *Woods et al*. [2008]
Matrosov et al. [2009] W08C	48	1.45	SSD data set: *Woods et al*. [2008]

[a]SSD, snowflake size distribution.

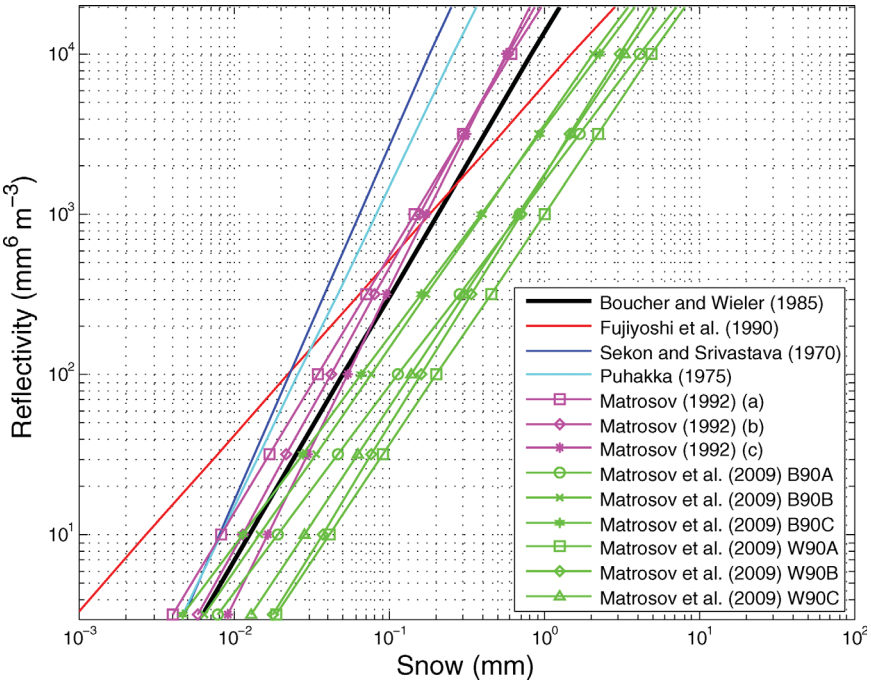

Figure 4. Reflectivity to snowfall rate (Z_H-S) relations. The different colors represent the diverse relations found in the literature. Highlighted in black is the *Boucher and Wieler* [1985] relation used in this study.

corresponded to the first elevation scan that did not contain strong clutter contamination, and it ranged from 300 to 600 m above the ground in the Wannengrat area. Due to its high elevation and in order to avoid overshooting precipitating systems, the analysis of the radar data is limited to a 10 km range.

2.5.2. Peaks and Valley *D*omains

[19] In order to investigate the effects of the processes related to topographically induced wind on snowfall, another set of subdomains was selected. Two disjointed areas were chosen based on the difference in altitudes between the DEM and the radar beam elevation at 9°. The first subdomain ("peaks") corresponds to a difference in elevations that ranges from 95 to 500 m and is mainly located close to the ridge. This area is expected to be strongly affected by the wind and turbulence caused by its proximity to the rugged terrain and the small-scale topographic features. The second subdomain ("valley") corresponds to differences in elevations that ranges between 700 and 1200 m. This domain is located predominantly far from the ridges (over the Davos valley), and it is supposed to be much less affected by turbulence and/or drifts (airflows) generated by the terrain.

[20] Both subdomains are presented in Figure 6: the peaks subdomain has an area of 4.9 km^2 (a), and the valley subdomain has an area of 7.6 km^2 (c; see also Figure 1). On the right-hand side of the plot, the radar beam elevation at 9° is presented for each of the new subdomains. The only subdomain that does not present clutter contamination at 0° is the valley subdomain. Its inclusion in the study corresponds to its proximity to the ground (ranges from 200 to 600 m, similar to the peaks subdomain at 9°), and its location far for the ridges (similar to the valley subdomain at 9°).

3. Data Analysis

3.1. (Semi)variograms

[21] The analysis of the spatial variability of snow accumulation measured on the ground and of the total amount

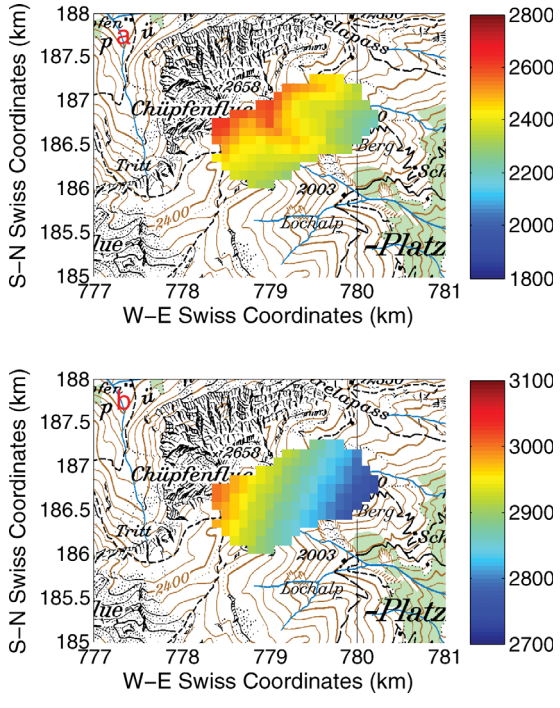

Figure 5. The lee-W subdomain used in the analysis: (a) altitude above sea level (m) for the lee-W subdomain of analysis obtained from the DEM and (b) radar beam altitude over the same subdomain.

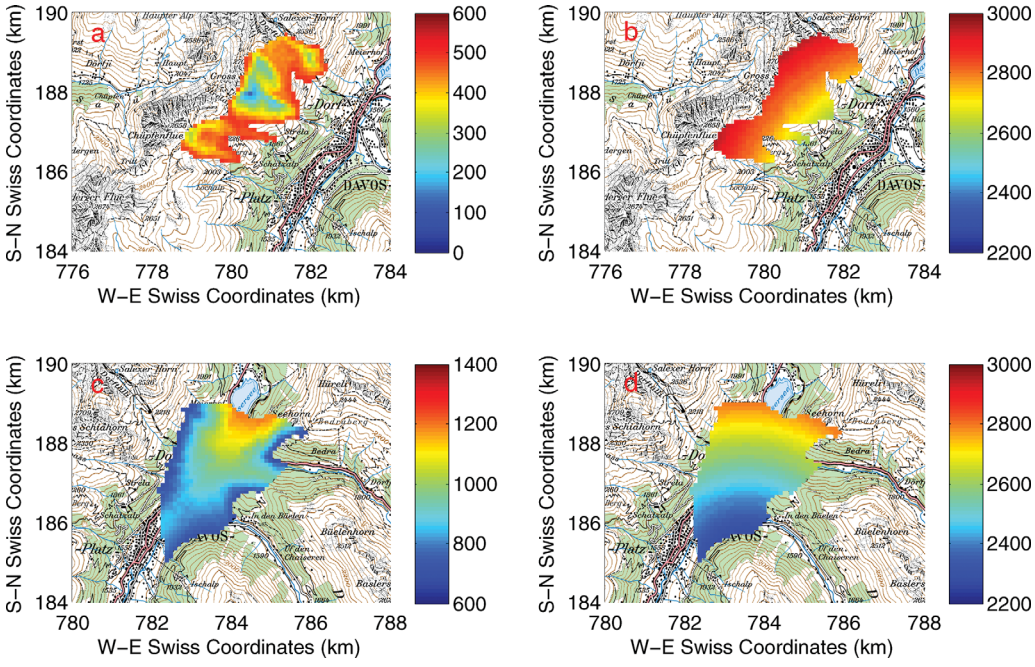

Figure 6. The peaks and valley subdomains: (a) relative altitude between the radar beam at 9° and the DEM in the peaks subdomain in which the difference between both elevations is less than 500 m; (b) radar beam height above the peaks subdomain; (c) relative altitude between the radar beam and the DEM in the valley subdomain. Here the difference between both quantities is selected between 700 and 1200 m; and (d) radar beam altitude over the valley subdomain.

of snowfall estimated by the radar is based on spatial (semi)variograms. The variogram is a key tool used in geostatistics to quantify the spatial structure of a random function [*Goovaerts*, 1997; *Chilès and Delfiner*, 1999]. The variogram $\gamma(\mathbf{h})$ measures the dissimilarities of the random function z values separated by a vector $\mathbf{h}$ as

$$\gamma(\mathbf{h}) = \frac{1}{2}\mathrm{E}\left\{[z(\mathbf{x}+\mathbf{h}) - z(\mathbf{x})]^2\right\}, \tag{3}$$

where E represents the expectation, and $\mathbf{x}$ is the position vector. When estimating the variogram from observations exhibiting symmetrical probability density functions, like in this study (not shown), the variogram is approximated by the "Matheron" estimator, which is an average function over the number of available pairs $N(\mathbf{h})$ as

$$\hat{\gamma}(\mathbf{h}) = \frac{1}{2N(\mathbf{h})}\sum_{i,j\in S_h}\left[z(\mathbf{x}_i) - z(\mathbf{x}_j)\right]^2, \tag{4}$$

where S_h is a subset of $N(\mathbf{h})$ points so that $\mathbf{x}_i - \mathbf{x}_j = \mathbf{h}$ with a given tolerance.

[22] For better comparison between the variograms obtained from the total amount of snowfall estimated by the radar and the snow accumulation measured at the ground, normalized (or climatological) variograms are considered [*Bastin et al.*, 1984]. The normalization of the variograms is obtained by dividing the estimator by the variance of the data under consideration, and the normalized variogram is dimensionless and has values ranging from zero to one. The variance of the data is estimated by

$$\hat{\mathrm{var}}\,(\mathbf{x}) = \frac{\sum_{i=1}^{M}[z(\mathbf{x}_i) - \bar{z}]^2}{M-1}, \tag{5}$$

where M is the number of points considered in the subdomain, and the overbar represents the arithmetic mean. When combining both expressions, the normalized variogram is expressed as

$$\hat{\gamma}(\mathbf{h}) = \frac{1}{2N(\mathbf{h})\hat{\mathrm{var}}\,(\mathbf{x})}\sum_{i,j\in S_h}\left[z(\mathbf{x}_i) - z(\mathbf{x}_j)\right]^2. \tag{6}$$

[23] The sample variance calculated according to equation (6) can underestimate the true variance, which leads to normalized variograms slightly larger than one.

3.2. Radar Measurements

[24] Radar data at 0° and 9° of elevation were analyzed for the whole period over which the radar was deployed in Davos. Winter events with no melting layer visible in the radar data (i.e., pure snow events) were selected. The selection of the events was confirmed by ground instruments located in the Weissfluhjoch Versuchsfeld area [*Stössel et al.*, 2010; *Mott et al.*, 2011a], which is located approximately 1 km away from the Wannengrat area. Additionally, no attenuation in the snowfall is considered because the maximum distance under analysis is 10 km from the radar location, and specific attenuation is limited in dry snow [e.g. *Battan*, 1973].

[25] The noise level in the radar signal was estimated at each radial considering only the gates with lower power

following an adaptation of the method of *Hildebrand and Sekhon* [1974]. The radar data were censored using a signal-to-noise ratio (SNR) of 5 dB. The selection of the SNR threshold guarantees that most of the low signal data are removed. Additionally, a simple hydrometeor classification scheme following the method described by *Shuur et al*. [2003] and *Park et al*. [2009] and adapted to X-band by *Snyder et al*. [2010] was implemented to remove any GC echoes and/or side lobes returns. Any remaining GC echoes, if any, were in addition manually removed before any further analysis.

[26] Radar data were obtained in polar coordinates with approximately 1.1° angular resolution and 75 m range resolution (see Table 1). However, the 3 dB beam width is 1.45°. As a consequence, all the data were resampled with 1.5° angular resolution in order to avoid angular smoothing and oversampling.

[27] Snow accumulation measurements in the Wannengrat subdomain are provided in the Swiss Cartesian coordinates. Taking that into consideration and the fact that the average distance from the radar to the lee-W subdomain is approximately 4 km, the radar data were resampled to a 100×100 m^2 grid in both north–south and east–west directions to avoid any additional smoothing of the data. The results of the resampling can be clearly observed in Figure 3, where the missing points at large ranges are a consequence of nonsmoothing.

[28] The resampled instantaneous reflectivity data Z_H (mm^6 m^{-3}) obtained approximately every 5 min at 9° elevation can now be converted to snowfall rate S (mm h^{-1}) using the *Boucher and Wieler* [1985] *Z-S* relation:

$$Z_H = 229S^{1.65}. \tag{7}$$

[29] The total snowfall amount estimates presented are obtained by adding the instantaneous snowfall estimates at each of the different domains over the periods of analysis.

[30] The mean Doppler radar velocity v_r and the Doppler spectral width data σ_v were censored following the same criteria of SNR threshold, and GC removal as Z_H. For most of the events in the winter of 2009/2010, v_r data are aliased due to configuration parameters: initially, single pulse pair (SPP) mode with unambiguous velocity of 6 m s^{-1}, and later SPP mode with unambiguous velocity of 16 m s^{-1}. No meaningful analysis of v_r and σ_v is possible in this period. In the summer 2010, a new configuration using double pulse pair (DPP) mode was implemented with an unambiguous velocity of 32 m s^{-1}.

3.3. Snow Accumulation

[31] Snow accumulation data obtained from ALS for the winters of 2007/2008 and 2008/2009 were acquired with 1 m grid resolution. The data were resampled at different grid resolutions to study the effect on spatial variability when decreasing the grid resolution. Additionally, at the time of the peak in snow accumulation, the density of the snow cover can be reasonably assumed constant [*Grünewald et al*., 2010; *Egli et al*., 2011], which allows the comparison of snow accumulation with total snowfall amount (expressed in millimeter of equivalent liquid water). The resampled snow accumulation data are now used to compute the normalized variogram with a maximum lag of 700 m. Normalized variograms of snow accumulation in the lee-W subdomain at 10 and 100 m resolutions for both winters are presented in Figure 7. Both variograms at 10 m present similar variability over the two winter seasons at all lags. The change in slope for both seasons is located at lags lower than 75 m. These results confirm the interannual consistency results of *Schirmer et al*. [2011] and *Deems et al*. [2008]. The variograms presented in this study complement those of *Mott et al*. [2011b] by providing variogram values for larger distance lags ($h > 100$ m).

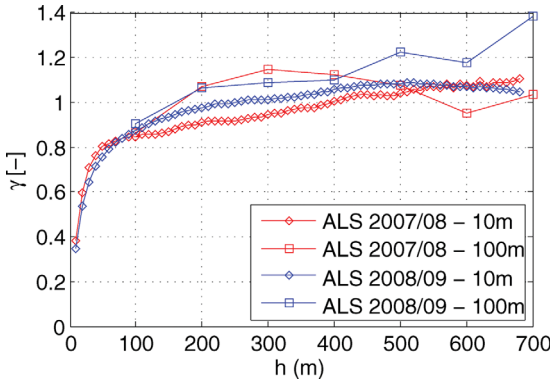

Figure 7. Normalized variograms of snow accumulation measured from ALS for the periods of 2007/2008 and 2008/2009. The 10 m resolution is denoted with diamonds, and the 100 m resolution is denoted with squares.

[32] The normalized variograms at 100 m (same grid resolution as the radar data) are similar until 400 m. The discrepancies observed at larger lags ($h > 400$ m) are caused by the reduced coverage of the subdomain (approximately 55%, see Figure 2) in the winter of 2007/2009 compared to the winter of 2008/2009. In both seasons at 100 m, the change in slope located at approximately 75 m is not captured. The normalized variograms at 10 and 100 m are in good agreement.

4. Results

4.1. Variability of Total Snowfall from Radar and Snow Accumulation

[33] The analysis of the variability is first focused on the lee-W subdomain. The total snowfall estimated from the radar reflectivity fields is presented in Figure 8a. The total snowfall amount ranges between 950 and 1100 mm. When these estimates are compared with the ones measured at the Weissfluhjoch station (Table 2), there are large differences but the order of magnitude is correct. These differences are due to possible effects of wind and evaporation but mainly to the fact that a constant Z_H-S relationship was used throughout the winter. This has however no significant impact on the global variability of snowfall (various Z_H-S relationships have been tested) which is the focus of the present study.

[34] The comparison of the total snowfall amount with the radar beam height of the same subdomain (Figure 5b) presents a dependency (see scatterplot in Figure 8b) with a correlation of $\rho = 0.6$. The correlation between these two quantities can be attributed to overshooting by the radar as winter precipitation often has limited vertical extension.

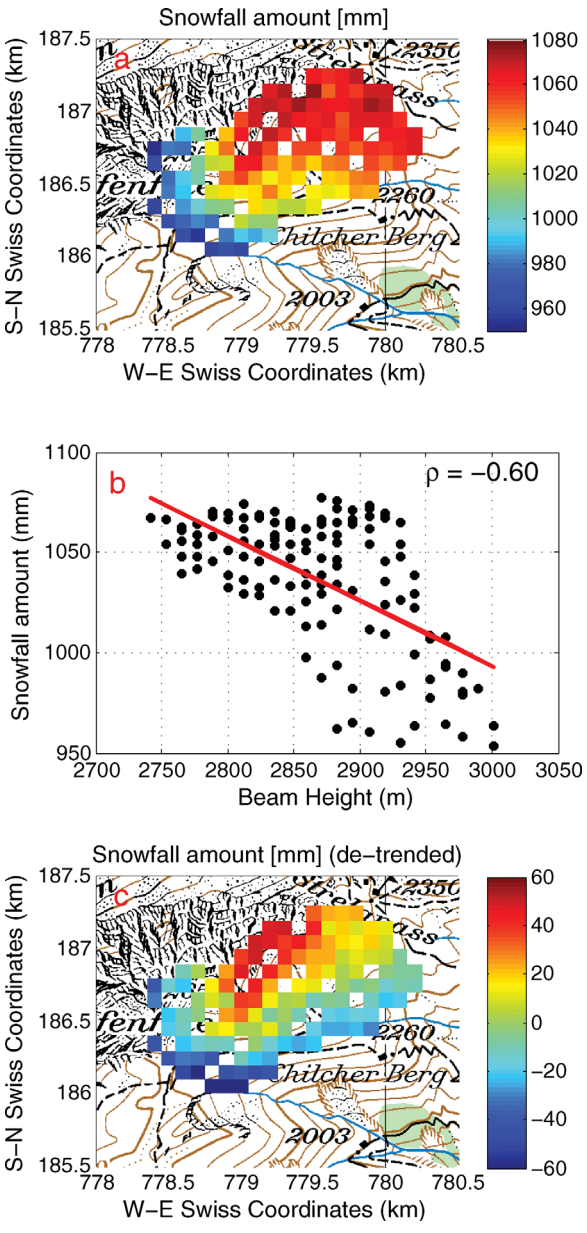

Figure 8. (a) Total snowfall amount (mm) for the winter season 2009/2010 estimated from the reflectivity fields. (b) Scatterplot between total snowfall amount and radar beam altitude. (c) Detrended snowfall amount fields used for the computation of the variograms.

The observed drift was removed to avoid contamination in the estimation of the variograms, which leads to the detrended snowfall amount presented in Figure 8c. The detrended fields present negative values, which have no effect on the spatial variability. These fields were obtained for the winter season of 2009/2010 and the March 2011 event and were used to calculate their corresponding normalized variograms.

[35] The variogram of snow accumulation obtained from ALS measurements for the lee-W subdomain is presented in Figure 9. As previously discussed in section 3.3, the difference in snow coverage from the winters of 2007/2008 and 2008/2009 causes the discrepancies between the ALS normalized variograms (h >400). The total snowfall accumulation normalized variograms for the different periods of study are also presented in Figure 9. The first period corresponds to the whole winter season of 2009/2010 and is presented in red. The second period corresponds to the single event between 17 and 20 March 2011 (Mar. 2011) and is presented in black. This period was selected because it deposited a large amount of snow (49 mm of snowfall water equivalent measured at the Weissfluhjoch, see Table 2) and because a predominant NW wind was observed during the whole event. The excellent agreement between the normalized variograms for the two periods shows that the spatial variability in total snowfall is consistent over the two studied periods (over the considered domain, at least), despite the difference in the number of snow events and in the quantity of snow they deposit on the ground. This confirms the strong influence of the NW winds in the spatial distribution of total snowfall in the area.

[36] The discrepancies found between the snow accumulation variograms from ALS and the total snowfall variograms are a clear indication that the snowfall observed through the radar reflectivity field exhibits a smoother spatial variability than the spatial snow accumulation patterns. The difference in altitude between the terrain and the radar beam at 9° ranges between 300 and 600 m (see Figure 5). The dissimilarities in the spatial structure between total snowfall and snow accumulation is interpreted as a signature of the fact that the main processes governing snow accumulation take place close to or at the surface and (possibly) at different times.

[37] An important contribution of the present paper is to show that by considering spatially distributed snowfall, the small-scale variability of snow depth on the ground cannot be explained by the snowfall variability because additional wind-induced processes control snow distribution on the ground. This is a useful experimental complement to the results from *Mott et al*. [2011b] based on a combination of local wind and snow depth measurements, Advanced Regional Prediction System (ARPS), and Alpine3D models.

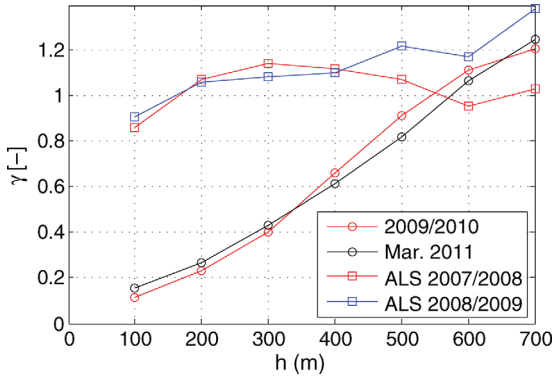

Figure 9. Normalized variograms obtained from the lee-W subdomain for different periods. Variograms from snow accumulation (ALS) from the winters of 2007/2008 and 2008/2009 are compared with the detrended total snowfall amount field variograms on different periods.

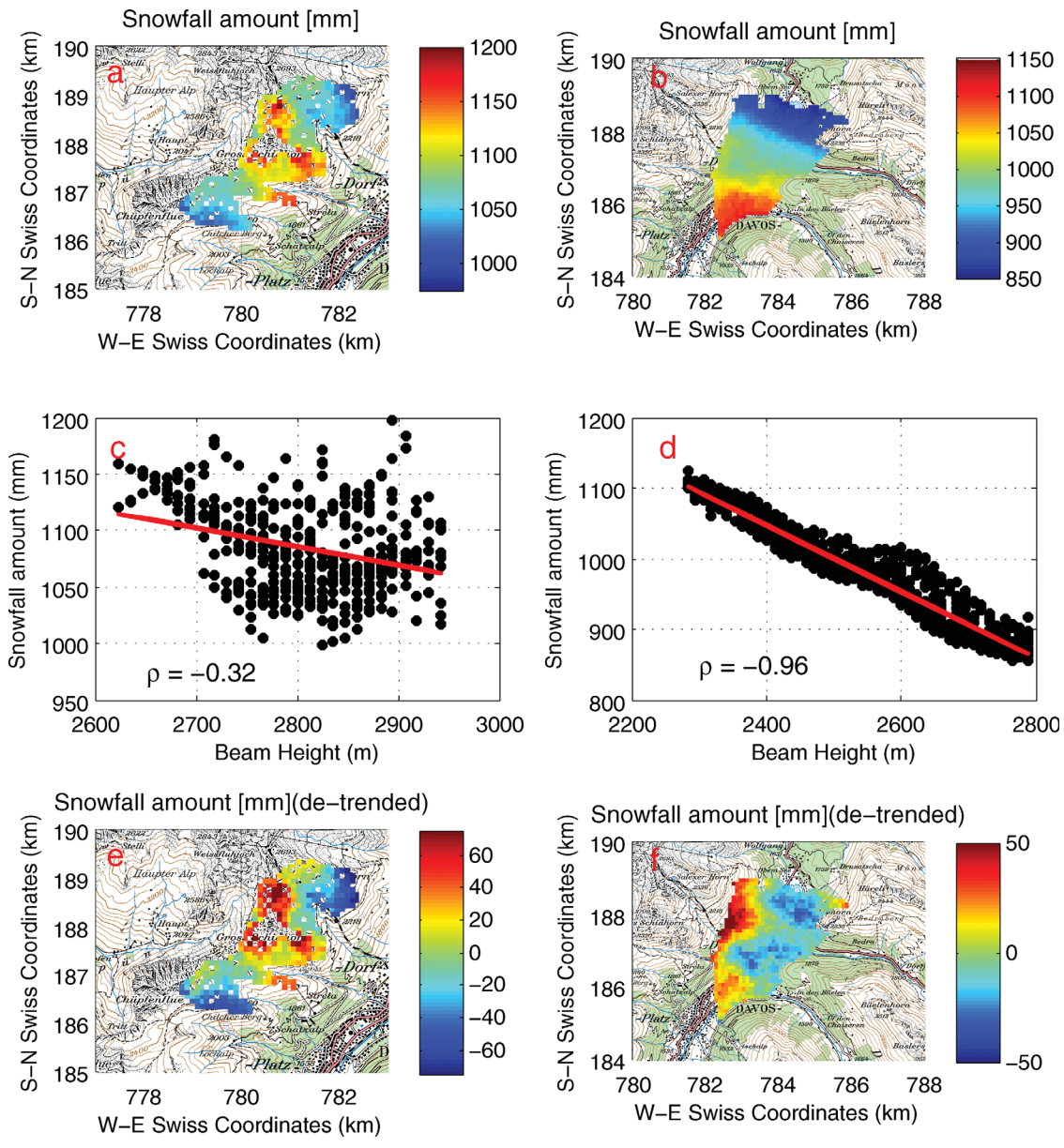

Figure 10. (a) Total snowfall amount (mm) obtained for the winter season of 2009/2010 for the peaks subdomain. (b) Total snowfall amount for the valley subdomain. (c) Scatterplot between total snowfall amount and radar beam height in the peaks subdomain. (d) Scatterplot between the total snowfall amount and radar beam height in the valley subdomain. (e) Detrended total snowfall amount in the peaks subdomain. (f) Detrended total snowfall amount in the valley subdomain.

4.2. Wind-Terrain Interaction

[38] A study of the influence of the wind-induced snow transport effect described in the previous section is conducted in this section through the analyses of spatial variability in the peaks and valley subdomains.

[39] For these two subdomains, variograms were calculated following the same procedure as before. Total snowfall amount retrieved from radar reflectivity was calculated for the winter season 2009/2010 and the event of March 2011 for both subdomains. The total snowfall amount retrieved for the winter season 2009/2010 is presented in Figures 10a and 10b for peaks and valley, respectively. Scatterplot between the radar beam height at 9° and total snowfall amount is presented in Figures 10c and 10d. Correlation observed at the peaks subdomain is low ($\rho = 0.32$), while correlation in the valley subdomain is much higher ($\rho = 0.96$). The high correlation observed in the valley indicated the overshooting of snow precipitation at high elevations above the ground. The detrended total snowfall amount fields are presented in Figures 10e and 10f.

[40] The detrended total snowfall amount fields are then used to calculate the variograms. Note that in this case, they are not the normalized variograms as in the case of the lee-W subdomain because they are computed from the same variable

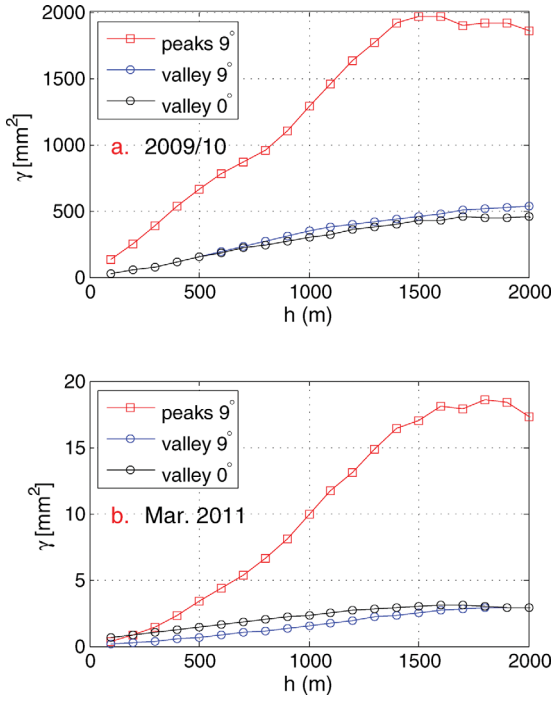

Figure 11. Variograms of snowfall amount obtained from the peaks and valley subdomains: (a) winter season of 2009/2010 and (b) event of March 2010. Variograms in the peaks subdomain are represented with squares while in the valley subdomain are presented in circles.

(total snowfall amount). Variograms for both subdomains and for both periods are presented in Figure 11.

[41] The variograms in the peaks domain is consistently higher (with a steeper slope) than in the valley subdomain for both winter periods. This shows that the spatial variability in the total snowfall amount is higher in the peaks subdomain. We suggest that this larger variability can be attributed to processes occurring close to the surface and induced by the local-scale topography.

[42] To further verify the influence of the topography, variograms of total snowfall amount at 0° in the valley subdomain are superimposed for both periods (see Figure 11 (black)). At this elevation, the difference between the elevations of the beam and the terrain is less than 600 m, so it is similar to the peaks subdomain. The roughness of the ground is however different, much lower in the valley subdomain (at 0°). The agreement at the valley subdomain at both elevations suggests that the rugged topography in the peaks subdomain has a strong influence on the spatial distribution of total snowfall amount than the altitude of the radar beam above the ground.

[43] To further analyze this behavior, the normalized histograms of the Doppler spectral width for both domains are analyzed for the March 2011 event (see Figure 12). The exclusion of the season 2009/2010 corresponds to data contaminated with strong velocity aliasing. The histograms corresponding to the peaks subdomain (at 9°) present larger mean values than the valley subdomain. However, when superimposing the histogram at 0° for the valley subdomain, the agreement with peaks from the 9° is remarkable. This suggests that the small-scale turbulence is stronger close to the surface where the winds are in direct contact with the terrain. Similar analysis for events in 2011 with lower wind speed (not shown) indicates that the spectral width is comparable at 0° and 9° in the valley domain.

[44] Finally, averaged normalized variograms of mean Doppler radial velocity are calculated for the March 2011 event, both subdomains, and both elevations. The use of the normalized variograms is to minimize the effects of the projection of the wind onto the radial to make possible the comparison between the peaks and the valley subdomains. The objective is to verify if the velocity field is more structured (in the systematic wind pattern) in the peaks domain, because of the small-scale topography, than in the valley subdomain, at comparable altitudes above the ground. The resulting variograms are presented in Figure 13. The ratio between the small-scale variability (i.e., nugget) and the total variance is lower at 9° in the valley and in the peaks subdomains than 0° in the valley subdomain. This shows a more organized structure of mean velocity fields than in the valley subdomain at 0°. This corroborates the important role of the topography in the spatial distribution of total snowfall.

[45] These combined findings quantitatively confirm that small-scale turbulence is stronger close to the surface where winds are in direct contact with the rugged terrain, and this strengthens the hypothesis that topographically induced winds strongly influence snow accumulation distribution, in agreement with the concept of preferential deposition proposed by *Lehning et al*. [2008].

5. Summary and Conclusions

[46] Various processes can influence the spatial distribution of snow depth on the ground. The main objective of the present study is to investigate the importance of the spatial variability of snowfall to explain the spatial variability of snow accumulation at the winter-season scale. These variabilities are quantified using variograms (normalized by the field sample variance) calculated over the Wannengrat area from which information on both quantities is available. Variograms of snow accumulation are obtained

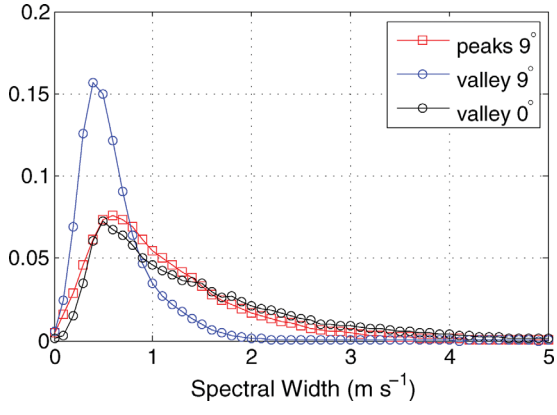

Figure 12. Histograms of the Doppler spectral width obtained from the peaks and valley subdomains for the event of March 2010. Histograms from the peaks subdomain are presented with squares, and the valley are presented with circles.

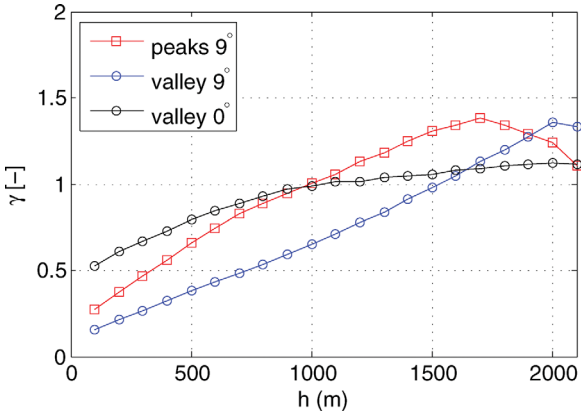

Figure 13. Variogram of Doppler radial velocity obtained from the peaks and valley subdomains for the event of March 2010. Variograms in the peaks subdomain are represented with squares while in the valley subdomain are presented in circles.

from ALS for winters 2007/2008 and 2008/2009 and confirm high interannual consistency in snow accumulation variability from one winter to the next [e.g. *Grünewald et al*., 2010; *Schirmer et al*., 2011; *Schirmer and Lehning*, 2011]. An X-band polarimetric radar collected measurements of the radar reflectivity Z_H. Total snowfall amount estimates were obtained from the radar reflectivity for the winter of 2009/2010 and from an intense snow event in March 2011.

[47] As expected, the comparison of the normalized variograms of total snowfall amount and of snow accumulation shows that the variability is much smoother in snowfall (a few hundred meters above the ground) than in snow accumulation. The similarity in the (normalized) variograms of total snowfall amount for the winter of 2009/2010 and for the March 2011 event is also noteworthy. This can be explained by the fact that intense snowfall mainly occurs during events with predominant NW winds. Because the radar beam is between 300 and 600 m above the ground in the study area, this difference in spatial variability is due to small-scale processes occurring close to the surface. To investigate the influence of the topographically induced wind patterns on snow accumulation, the spatial variability of total snowfall amount is analyzed in two subdomains defined by the relative altitude of the radar beam with respect to the terrain. The peaks subdomain corresponds to altitudes between 95 and 500 m in the vicinity of the slope, and the valley subdomain corresponds to altitudes between 700 and 1200 m. The variograms in the peaks subdomain show a larger variability than in the valley subdomain. This is confirmed through the analysis of the distribution of the spectral width, related to turbulence, in both subdomains. The peaks subdomain exhibits higher values than the valley subdomain, which indicates stronger turbulence caused by the rougher terrain.

[48] The analyses presented in this paper show that snowfall variability (at a height of a few hundred meters above the ground) is not the driving factor of snow accumulation variability at small scales (below a few kilometers), as the latter is additionally affected by snow redistribution processes and (indirectly) shows that topographically induced wind patterns have a dominant influence on snow accumulation. Such wind patterns also have a strong effect on the snow variability as seen in the different areas (peaks and valley). These results obtained from observations complement and confirm previous studies based on simulations [e.g., *Mott et al*., 2010, 2011b].

[49] The main limitation comes from the lack of radar measurements at lower elevation angles, which would allow the investigation of snowfall, as well as wind and turbulence closer to the ground level. This is a difficult issue because contamination of radar observations by GC will also increase close to the terrain. In addition, snow accumulation measurements from ALS were available over a rather limited area and for different winter seasons. Data for snow accumulation over larger areas and collected during the same winter seasons as radar data would also strengthen the analyses.

[50] In order to better understand the physics of the small-scale processes governing snowfall and snow accumulation variability in space and time, the combination of radar measurements and numerical weather model simulations will be conducted in future work. Finally, the present study focuses on the spatial variability over the winter season, so the behaviors of snowfall and snow accumulation are integrated over winter periods. Investigations at the event scale would be interesting, as various synoptic and local conditions can occur.

[51] **Acknowledgments.** This work is funded by the Swiss National Science Foundation under grants 200021-125064 and 200021-125332. Significant further funding has been obtained from the Competence Center of Environment and Sustainability (CCES) of the Eidgenössische Technische Hochschule (ETH) domain through the Swiss Experiment Project and the "Amt für Wald und Naturgefahren" (ALS flights). The authors also thank Nicholas Dawes from SLF for his help.

References

Bastin, G., B. Lorent, C. Duqué, and M. Gevers (1984), Optimal estimation of the average areal rainfall and optimal selection of rain gauge locations, *Water Resour. Res.*, *20*(4), 463–470.

Battan, L. J. (1973), *Radar Observation of the Atmosphere*, 324 pp., Univ. of Chicago Press, Chicago, Ill.

Bellaire, S., and J. Schweizer (2011), Measuring spatial variations of weak layer and slab properties with regard to snow slope stability, *Cold Reg. Sci. Technol.*, *65*(2), 234–241, doi:10.1016/j.coldregions.2010.08.013.

Birkeland, K. W., K. J. Hansen, and R. L. Brown (1995), The spatial variability of snow resistance on potential avalanche slopes, *J. Glaciol.*, *41*(137), 183–190.

Boucher, R. J., and J. G. Wieler (1985), Radar determination of snowfall rate and accumulation, *J. Clim. Appl. Meteorol.*, *24*, 68–73.

Braham, R. R. (1990), Snow particle size spectra in lake effects snows, *J. Appl. Meteorol.*, *29*, 200–207.

Chilès, J.-P., and P. Delfiner (1999), Geostatistics: Modeling Spatial Uncertainty, *Probability and Statistics*, 695 pp., John Wiley & Sons, Inc., New York.

Dadic, R., R. Mott, M. Lehning, and P. Burlando (2010), Parametrization for wind-induced preferential deposition of snow, *Hydrol. Processes*, *24*, 1994–2006, doi:10.1002/hyp.7776.

Deems, J., S. Fassnacht, and K. Elder (2008), Interannual consistency in the fractal snow depth patterns at two Colorado mountain sites, *J. Hydrometeorol.*, *9*(5), 977–988.

Doviak, R. J., and D. S. Zrnić (1993), *Doppler Radar and Weather Observations*, 2nd ed., Academic, San Diego, Calif.

Egli, L., N. Griessinger, and T. Jonas (2011), Seasonal development of spatial snow-depth variability across different scales in the Swiss Alps, *Ann. Glaciol.*, *52*, 216–222.

Evans, A. G., J. D. Locatelli, M. T. Stoelinga, and P. V. Hobbs (2005), The IMPROVE-1 storm of 1–2 February 2001. Part II: Cloud structures and the growth of precipitation, *J. Atmos. Sci.*, *62*(10), 3456–3473.

Fujiyoshi, T., T. Endoh, T. Yamada, K. Tsuboki, Y. Tachibana, and G. Wakahama (1990), Determination of Z-R relationship for snowfall using a radar and high sensitivity snow gauges, *J. Appl. Meteorol.*, *29*, 147–152.

Goovaerts, P. (1997), *Geostatistics for Natural Resources Evaluation*, *Appl. Geostat. Ser.*, Oxford University Press, New York.

Grünewald, T., M. Schirmer, R. Mott, and M. Lehning (2010), Spatial and temporal variability of snow depth and ablation rates in snow mountain catchment, *Cryosphere*, *4*, 215–225, doi:10.5194/tc-4–215-2010.

Hildebrand, P. H., and R. S. Sekhon (1974), Objective determination of the noise level in Doppler spectra, *J. Appl. Meteorol.*, *13*, 808–811.

Kennedy, P. C., and S. A. Rutledge (2011), S-band dual-polarization radar observations of winter storms, *J. Appl. Meteorol. Climatol.*, *50*, 844–858, doi:10.1175/2010JAMC2558.1.

Kneifel, S., M. Maahn, G. Peters, and C. Simmer (2011), Observation of snowfall with a low-power FM-CW K-band radar (micro rain radar), *Meteor. Atmos. Phys.*, *113*, 75–87, doi:10.1007/s00703-011-0142-z.

Lehning, M., H. Löwe, M. Ryser, and N. Raderschall (2008), Inhomogeneous precipitation distribution and snow transport in steep terrain, *Water Resour. Res.*, *44*, W07404, doi:10.1029/2007WR006545.

Lehning, M., T. Grünewald, and M. Schirmer (2011), Mountain snow distribution governed by an altitudinal gradient and terrain roughness, *Geophys. Res. Lett.*, *38*, L19504, doi:10.1029/2011GL048927.

Luce, C. H., D. G. Tarboton, and K. R. Cooley (1998), The influence of the spatial distribution of snow on basin-averaged snowmelt, *Hydrol. Processes*, *12*(10–11), 1671–1683.

Matrosov, S. Y. (1992), Radar reflectivity in snowfall, *IEEE Trans. Geosci. Remote Sens.*, *30*(3), 454–461.

Matrosov, S. Y. (1998), A dual-wavelength radar method to measure snowfall rate, *J. Appl. Meteorol.*, *37*, 1510–1521.

Matrosov, S. Y., C. Campbell, D. Kingsmill, and E. Sukovich (2009), Assessing snowfall rates from X-band radar reflectivity measurements, *J. Atmos. Ocean. Technol.*, *26*, 2324–2339, doi:10.1175/2009¥JTECHA1238.1.

Mitchell, D. L., A. Huggins, and V. Grubišić (2006), A new snow growth model with application to radar precipitation estimates, *J. Atmos. Res.*, *82*, 2–18, doi:10.1016/j.atmosres.2005.12.004.

Mott, R., M. Schirmer, M. Bayar, T. Grünewald, and M. Lehning (2010), Understanding snow-transport processes shaping the mountain snowcover, *Cryosphere*, *4*, 545–559, doi:10.5149/tc-4–545-2010.

Mott, R., L. Egli, T. Grünewald, N. Dawes, C. Manes, M. Bavay, and M. Lehning (2011a), Micrometeorological processes driving snow ablation in an Alpine catchment, *Cryosphere*, *5*, 1083–1098.

Mott, R., M. Schirmer, and M. Lehning (2011b), Scaling properties of wind and snow depth distribution in an Alpine catchment, *J. Geophys. Res.*, *116*, D06106, doi:10.1029/2010JD014886.

Park, H. S., A. V. Ryzhkov, D. S. Zrnić, and K.-E. Kim (2009), The hydrometeor classification algorithm for the polarimetric WSR-88D: Description and application to an MCS, *Weather Forecast.*, *24*(3), 730–748.

Pomeroy, J. W., P. Marsh, and D. M. Gray (1997), Application of a distributed blowing snow model to the artic, *Hydrol. Processes*, *11*(11), 1451–1464.

Puhakka, T. (1975), On the dependence of Z-R relation on the temperature in snowfall, paper presented at 16th Radar Meteorology Conference, Am. Meteorol. Soc., Huston, Tex.

Roe, G. H. (2005), Orographic precipitation, *Ann. Rev. Earth Planet. Sci.*, *33*, 645–671, doi:10.1146/annurev.earth.33.092203.122541.

Schirmer, M., and M. Lehning (2011), Persistence in intra-annual snow depth distribution: 2. Fractal analysis of snow depth development, *Water Resour. Res.*, *47*, W09517, doi:10.1029/2010WR009429.

Schirmer, M., V. Wirz, A. Clifton, and M. Lehning (2011), Persistence in inter-annual snow depth distribution: 1. Measurements and topographic control, *Water Resour. Res.*, *47*, W09516, doi:10.1029/2010WR009426.

Schneebeli, M., and A. Berne (2012), An extended Kalman filter framework for polarimetric X-band weather radar data processing, *J. Atmos. Ocean. Technol.*, *29*, 711–730, doi:10.1175/JTECH–D–10–05053.1.

Schneebeli, M., N. Dawes, M. Lehning, and A. Berne (2013), High resolution vertical profiles of X-band polarimetric radar observables during snowfall in the Swiss Alps, *J. Appl. Meteorol. Climatol.*, doi:10.1175/JAMC-D-12–015.1.

Schweizer, J., B. Jameison, and M. Schneebeli (2003), Snow avalanche formation, *Rev. Geophys.*, *41*(4), 1016, doi:10.1029/2002RG000123.

Sekhon, R. S., and R. C. Srivastava (1970), Snow size spectra and radar reflectivity, *J. Atmos. Sci.*, *27*, 299–307.

Shuur, T., A. Ryzhkov, P. Heinselman, D. Zrnić, D. Burgess, and K. Scharfenberg (2003), Observations and classification of echoes with the polarimetric WSR-88D radar, 46 pp., Rep. of the Nat. Severe Storms Lab., Norman, Okla. [Available at http://cimms.ou.edu/∼schuur/jpole/JPOLE_HCA_report_pdf.pdf.]

Snyder, J. C., H. B. Bluestein, G. Zhang, and S. J. Frasier (2010), Attenuation correction and hydrometeor classification of high-resolution, X-band, dual-polarized mobile radar measurements in severe convective storms, *J. Atmos. Ocean. Technol.*, *27*, 1979–2001, doi:10.1175/2010JTECHA1356.1.

Stössel, F., M. Guala, C. Fierz, C. Manes, and M. Lehning (2010), Micrometeorological and morphological observations of surface hoar dynamics on a mountain snow-cover, *Water Resour. Res.*, *46*, W04511, doi:10.1029/2009WR008198.

Swisstopo (2004), DHM25, the digital height model of Switzerland, Technical report. [Available at http://www.swisstopo.admin.ch/internet/swisstopo/en/home/products/height/dhm25.parsysrelated1.44518.downloadList.76700.DownloadFile.tmp/dhm25infoen.pdf.]

Woods, C. P., M. T. Stoelinga, and J. D. Locatelli (2008), Size spectra of snow particles measured in wintertime precipitation in the Pacific northwest, *J. Atmos. Sci.*, *65*, 189–205.

Zängl, G., D. Aulehner, C. Wastl, and A. Pfeiffer (2008), Small-scale precipitation variability in the Alps: Climatology in comparison with semi-idealized numerical simulations, *Q. J. R. Meteorol. Soc.*, *134*, 1865–1880, doi:10.1002/qj.311.